Hindawi Publishing Corporation
Journal of Sensors
Volume 2009, Article ID 980965, 7 pages
doi:10.1155/2009/980965

Research Article

Sb-SnO_2-Nanosized-Based Resistive Sensors for NO_2 Detection

T. Krishnakumar,[1] R. Jayaprakash,[1] N. Pinna,[2,3] A. Donato,[4] N. Donato,[5] G. Micali,[6] and G. Neri[6]

[1] *Nanotechnology Laboratory, Department of Physics, Sri Ramakrishna Mission Vidyalaya College of Arts and Science, Coimbatore, Tamilnadu-641 020, India*
[2] *Department of Chemistry, CICECO, University of Aveiro, 3810-193 Aveiro, Portugal*
[3] *World Class University (WCU) program of Chemical Convergence for Energy & Environment (C2E2), School of Chemical and Biological Engineering, College of Engineering, Seoul National University (SNU), Seoul 151-744, South Korea*
[4] *Department of Mechanics and Materials, University Mediterranea, 89100 Reggio Calabria, Italy*
[5] *Department of Matter Physics and Electronic Engineering, University of Messina, 98166 Messina, Italy*
[6] *Department of Industrial Chemistry and Materials Engineering, University of Messina, 98166 Messina, Italy*

Correspondence should be addressed to G. Neri, neri@ingegneria.unime.it

Received 17 December 2008; Accepted 30 April 2009

Recommended by Giorgio Sberveglieri

A study over Sb-promoted tin oxide nanopowders for sensing applications is reported. SnO_2 nanopowders pure and promoted with 5 wt% of antimony were prepared by wet chemical methods and widely characterized by TEM, XRD, and XPS techniques. Thick film resistive sensors were fabricated by depositing the synthesized nanopowders by drop-coating on interdigited alumina substrates. The sensing characteristics of the pure SnO_2 and Sb-promoted sensors for the monitoring of trace level of NO_2 were studied. The response of the sensors to water vapor was also investigated, revealing that Sb acts favorably eliminating the interference of humidity.

1. Introduction

Metal oxide semiconductors (MOSs) in the form of highly porous films are widely used in resistive chemical sensors for the monitoring of gaseous species in several applications of technological interest [1]. Tin oxide (SnO_2) is the most used sensing material in commercially sensor devices for toxic gases detection [2]. It is well known that the sensing properties of SnO_2-based material depend on its chemical and physical characteristics, which are strongly dependent on the preparation conditions, dopant and grain size. This implies that the synthesis of the sensing material is a key step in the preparation of high-performance MOS gas sensors.

SnO_2 powders and films can be prepared by a variety of synthesis methods [3–8]. Furthermore, the electrical and sensing properties of the undoped tin oxide can be modulated by addition of proper amounts of suitable dopants. For example, promoting SnO_2 with antimony, the electrical properties can be enhanced in order to greatly reduce the resistivity of the sensing film [9, 10]. This is particularly advantageous specially at low temperature, because in this temperature interval the electrical resistance of SnO_2 films is generally high and complicates the measurements with conventional instruments.

Grain size reduction is another of the main factors for enhancing the gas sensing properties of semiconducting oxides [11–13]. It is believed that improved sensing technologies can be configured and developed by taking advantage of recent advances in nanosized materials. They are currently receiving a great deal of attention due to their unique physical properties, which derive from their nanometer-scaled sizes. In such materials, for example, the surface-to-bulk ratio is much greater than coarse materials, so that the surface properties become paramount, which makes them particularly appealing in applications, such as gas sensors, where nanosized properties can be exploited. In this regards, pure and promoted SnO_2 nanocrystalline powders have attracted much attention because of their promising applications in practical sensor devices [14, 15].

Aim of this work is to develop a nitrogen dioxide (NO_2) sensor device based on SnO_2 nanopowders with particularly low cross-sensitivity to humidity. NO_2 is a major

Table 1: Main characteristics of the nanopowders synthesized and treated at different temperatures.

Code	Sb (wt%)	Treatment temperature (°C)	Crystallyne structure	Mean grain size (nm)
SnO_2	0	120	SnO, Tetragonal	26
		300	SnO_2, Cassiterite	29
		600	SnO_2, Cassiterite	31
Sb-SnO_2	5	120	SnO	12
		300	SnO_2, Cassiterite	15
		600	SnO_2, Cassiterite	16

atmospheric pollutants causing acid rains and photochemical smog. Therefore, nowadays the more and more strict regulations on the emission of this toxic gas require fast and accurate detection of NO_2 at sub-ppm concentration. The development of semiconductor sensors for detecting NO_2 in air is then strongly demanding. Previous sensor devices based on tin oxide have been described in literature [16–18]. However, humidity effects on these sensors are relevant and can significantly affect performance and cause false alarms.

For this scope here we focused our attention on Sb-SnO_2 nanopowders, with aim to develop a sensor sensitive to nitrogen dioxide at low concentrations and with a humidity-independent character. Results of previous detailed characterizations by XRD, TEM, and XPS of the synthesized nanopowders [19, 20] were taken into account in order to correlate the microstructural properties with the sensing characteristics. Performances of the Sb-SnO_2 sensor were also compared with that of a reference sensor based on nanosized pure SnO_2 powders.

2. Experimental

2.1. Nanopowders Synthesis. Reference pure SnO_2 nanopowders were synthesized as follows. A 0.1 M solution of tin(II) chloride in deionized water was prepared. Then pH of the solution was maintained between 7 and 9 using liquid ammonia diluted with water. The resulting precipitate was washed with water until no chlorine ions are detected and further washed with ethanol to remove NH_4^+ ions. The resulting precipitate was irradiated at a frequency of 2.45 GHz and power up to 1 kW in a microwave oven for 10 minutes.

The Sb-SnO_2 nanopowders were synthesized by a chemical precipitation technique. The appropriate amount of $SbCl_3$ in order to have a nominal 5 wt% in the Sb-SnO_2 powder was dissolved first in fuming HCl. The resulting clear solution was added dropwise into 0.1 mol $SnCl_2 \cdot 2H_2O$ (98%, Merck chemicals) of solution using water as solvent. The total solution was stirred for 30 minutes, and aqueous phase ammonia (25%) was added dropwise until the pH of the solution adjusted to 4. Within few seconds a white precipitate was obtained. It was washed with water and ethanol until no chlorine ions were detected and refluxed for 12 hours. The refluxed precipitate was filtered and dried at 120°C in air, and the residue was ground to fine powder in a mortar and pestle.

In order to characterize the thermal behavior of the as prepared SnO_2 and Sb-SnO_2 nanopowders, they were sintered at different temperatures (up to 600°C) in air for 5 hours at a rate of 5°C/minutes. Main characteristics of the nanopowders are reported in Table 1.

2.2. Nanopowders Characterization. XRD measurements were performed on a Bruker AXS D8 Advance instrument using the CuKα with wavelength of 1.541 Å. The average crystalline size of the nanoparticle was evaluated using the Scherrer formula

$$d = \frac{K\lambda}{\beta \cos\theta}, \tag{1}$$

where d is the mean crystalline size, K is a grain shape dependent constant (0.9), λ is the wavelength of the incident beam, θ is a Bragg reflection angle, and β is the full width half maximum. Transmission Electron Microscopy (TEM), Selected-Area Electron Diffraction (SAED), and Energy Dispersive Spectroscopy (EDS) were recorded on a Technai G20-stwin Higher Resolution Electron Microscope (HRTEM) using an accelerating voltage of 200 kV. The X-Ray Photoelectron Spectroscopy (XPS) analyses have been performed using the PHI ESCA system equipped with an Mg X-ray source (h = 1253.6 eV) with a hemispherical analyzer.

2.3. Sensing Tests. Sensors were made by depositing by drop coating films (1–10 μm thick) of the nanopowders dispersed in water on alumina substrates (6×3 mm^2) with Pt interdigitated electrodes and a Pt heater located on the backside. A schematic picture of the sensor structure and a photo of one fabricated sensor device are reported in Figure 1. The sensors were then introduced in a stainless-steel test chamber for the sensing tests. The experimental bench for the electrical characterization of the sensors (Figure 2) allows to carry out measurements in controlled atmosphere. Gases coming from certified bottles can be further diluted in air at a given concentration by mass flow controllers. Electrical measurements were carried out in the temperature range from 50 to 250°C, with steps of 50°C, under a dry air total stream of 200 sccm, collecting the sensors resistance data in the four-point mode. A multimeter data acquisition unit Agilent 34970A was used for this purpose, while a dual-channel power supplier instrument Agilent E3632A was employed to bias the built-in heater of the sensor to perform measurements at superambient temperatures.

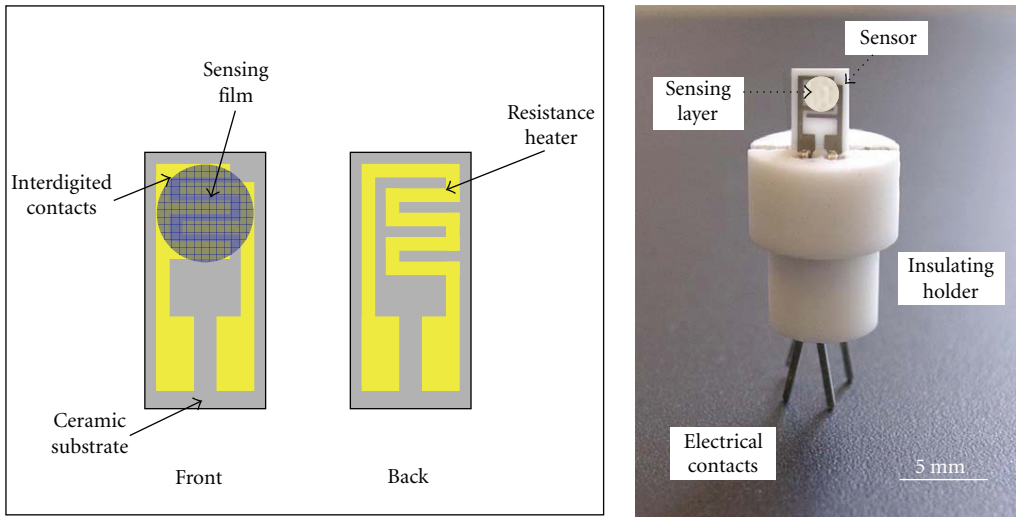

Figure 1: Schematic representation of the sensor architecture and photograph of the fabricated sensor device.

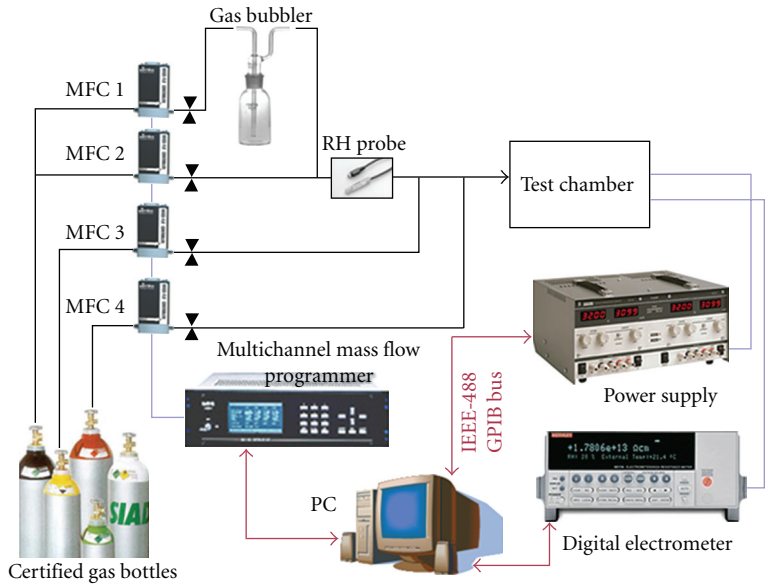

Figure 2: Experimental setup for gas sensors characterization.

The gas response, S, is defined as $S = R/R_0$ where R is the electrical resistance of the sensor at different NO_2 concentrations in dry air and R_0 the resistance in dry air.

Humidity tests were carried out in the range of 0%–100% RH. The different RH values were obtained by mixing dry and wet air (coming from a bubbler maintained at 20°C) into opportune volumetric ratios.

3. Results and Discussion

3.1. Microstructural Characterization. A detailed characterization of the nanopowders under study has been reported elsewhere [19, 20]. Here we recall briefly some data important for the present application. The analyses carried out on the "as prepared" materials showed that the main crystalline phase is SnO. Increasing the calcination temperature, the microstructure evolved stably up to SnO_2. The pure SnO_2 sample sintered at 600°C showed typical SnO_2 tetragonal Cassiterite reflections, with the calculated lattice parameters of tin oxide nanoparticles ($a = 0.483$ nm, $c = 0.325$ nm) in good agreement with the standard values ($a = 0.474$ nm, $c = 0.319$ nm). The average particle size, as estimated from XRD measurements, increases slightly with the treatment temperature (from 26 to 30 nm after calcination at 600°C).

Similar findings have been found on the Sb-promoted tin oxide nanopowders. On the sample sintered at 600°C, XRD analysis (Figure 3) indicated the existence of tetragonal Cassiterite type of Sb-substituted SnO_2 crystals, implying that all antimony ions came into the crystal lattice of bulk SnO_2 to substitute for tin ions. Calculation through the

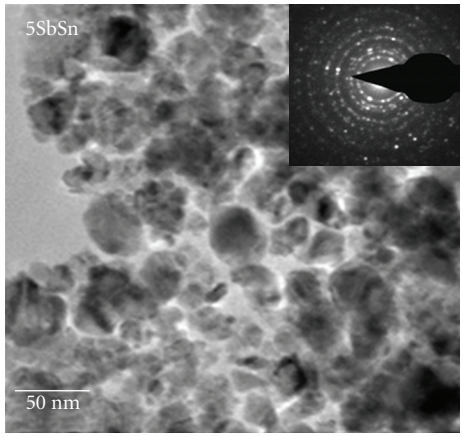

Figure 3: XRD characterization of the Sb-SnO_2 nanopowders treated at 600°C. Plane index related to SnO_2 Cassiterite is shown.

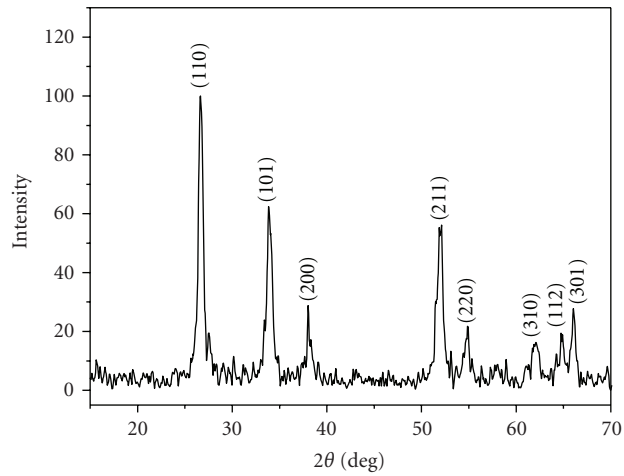

Figure 4: TEM characterization of the Sb-SnO_2 nanopowders treated at 600°C.

Scherrer formula indicated that the average particle size of 5 wt% antimony promoted tin oxide powder sintered at 600°C is in the range of 20 nm.

Typical morphology of the Sb-promoted tin oxide nanopowders treated at high temperature (600°C) is shown in the TEM micrograph in Figure 4. The corresponding SAED pattern is also reported in the insert. The particle size estimated from TEM measurements corresponds to the average size (20 nm) evaluatedfrom XRD measurements, suggesting that they should be monocrystalline.

In order to investigate the stoichiometry of the 5 wt% Sb-SnO_2 nanopowders, a detailed XPS analysis has been carried out. At this concentration of antimony, the Sb^{5+} component was found to be dominant with only a small amount of Sb^{3+} content [20]. Due to the substitution of Sb^{5+} ion by replacing Sn^{4+} ion, the donor center was appeared very close to the conduction band of SnO_2; that is, donor level was merging with conduction band. This has reflected a decrease in the resistance of the sample.

From characterization data above reported and summarized in Table 1, it can be deduced that crystalline characteristics of SnO_2 were not affected by promoter addition. On the contrary, the grain size was largely dependent on the addition of Sb. Thus, the Sb-promoted powders have presented lower grain size with respect to the unpromoted one. This is in agreement with results reported by other authors [21]. Even if an absolute comparison cannot be made because the samples derive from different preparation methods, this behavior can be explained by the blocking effect of the Sb atoms on the grains growth.

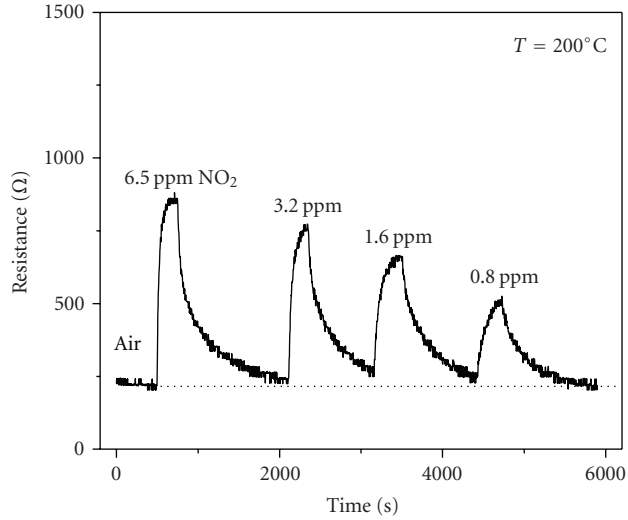

Figure 5: Transient response of the Sb-SnO_2 sensor operated at 200°C to different NO_2 concentrations.

3.2. NO_2 Sensing Tests. To perform sensing tests, sensor devices were fabricated depositing by drop coating the synthesized nanopowders on interdigited alumina substrates, as described in the experimental section. The as synthesized SnO_2 and Sb-SnO_2 nanopowders resulted particularly suitable for deposition without the use of any further additive. After the sensing layer was deposited on the ceramic substrate, a high-temperature treatment was performed in order to stabilize the film microstructure.

Electrical measurements have shown, as expected, that the baseline resistance of Sb-promoted sensor in air is lower than measured for the pure SnO_2-based sensor. A low resistance of the sensing layer is a favorable factor implying a low noise in the measurement of the resistance and consequently a high signal/noise ratio. The low resistance of the Sb-SnO_2 film can be explained considering that SnO_2 is a metal oxide with *n*-type semiconducting behavior. In the presence of Sb^{5+}, the SnO_2 conductivity increase can be due to the formation of holes.

Figure 5 shows a typical transient response to different NO_2 concentrations obtained with the Sb-SnO_2 sensor operated at 200°C. The sensing layer was in this case pretreated at 300°C. The responses are fast and reversible. The response time, τ_{res}, defined here as the time it takes for the resistance of the gas sensor to decrease to 90% of the minimum resistance when NO_2 is introduced into air, is fast ($\tau_{res} < 90$ seconds). The recovery time, τ_{rec}, the

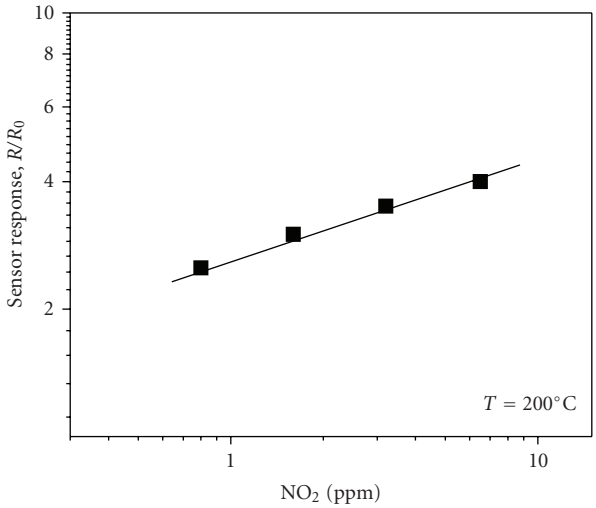

Figure 6: Response of the Sb-SnO_2 sensor as a function of the NO_2 concentration.

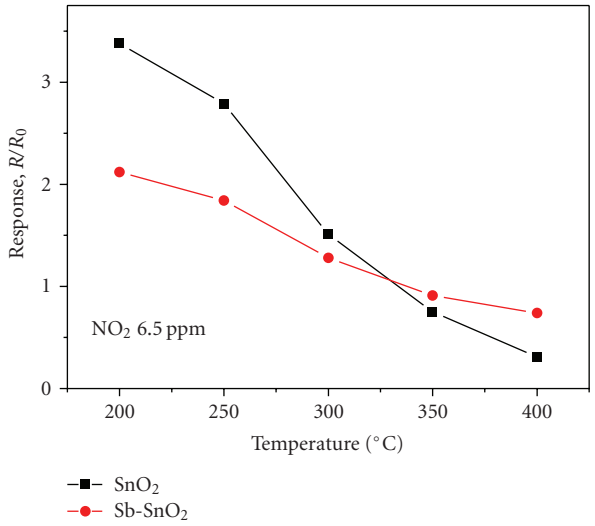

Figure 7: Response of the SnO_2 and Sb-SnO_2 sensors as a function of the operating temperature.

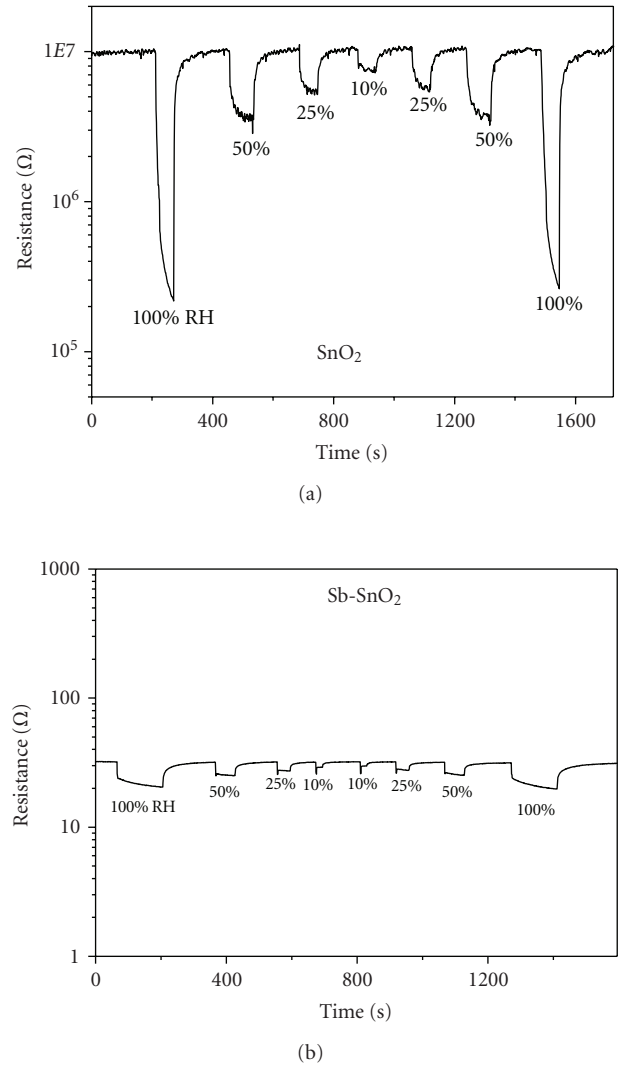

Figure 8: Dynamic response of the SnO_2 and Sb-SnO_2 sensors at the operating temperature of 200°C to step changes in relative humidity levels.

time required for 90% increment in resistance when NO_2 is turned off and air is reintroduced into the chamber, is instead longer. The response of the sensor correlate linearly with the concentration of the gas target (Figure 6). The good response to 0.8 ppm of NO_2 indicates the promising performance of the sensor for the detection of sub-ppm concentrations of nitrogen dioxide in air.

Tests carried out with sensing layer treated at higher temperatures have shown that the response slightly decreases. This can be attributed to a loss of surface area consequently to grain size increment. However, treatment temperature at least up to 400°C is necessary in order to stabilize the microstructure of the sensing layer, its grain size, and the adhesion to the substrate. Indeed, after thermal treatment, the adhesion of the sensing layer to the alumina substrate was found to be very tight and durable to stretch. Therefore, further sensing tests have been carried out with pretreatment temperature of 400°C.

Tests aimed to find the optimal operating temperature of the sensors for NO_2 monitoring are reported in Figure 7. The operative range investigated was between 200 and 400°C. The lower limit was related to the necessity to provide an adequate fast response/recovery time. At all operating temperatures, the pure SnO_2 sensor showed a larger response compared to Sb-promoted sensor. It was also observed that at operating temperature higher than 300°C the sensor response is lower than 1 (i.e., the resistance in nitrogen dioxide is lower that registered in air). This can be explained on the basis of a transition from n- to p-type response, as observed for different metal oxide semiconductors exposed to various gases [22], leading in our case to an inverse response above 300°C. A more detailed investigation is however necessary in order to better understand the above observed behavior.

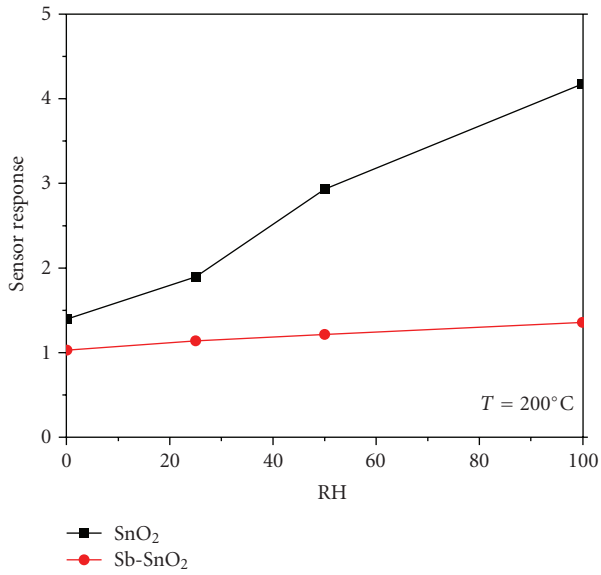

FIGURE 9: Magnitude of signal increases versus RH for both sensors investigated.

Taking into account all sensing characteristics (sensitivity, response/recovery time) and power consumption, the working temperature of 200°C provides the better opportunity for the sensor operation. Despite antimony addition worsens the response toward NO_2, it acts favorably eliminating the interference of humidity. In this regard, analyzing the response to different mixtures of NO_2 and RH, no influence of the water vapor on the NO_2 sensor response was observed.

3.3. Humidity Tests. It is well known that tin dioxide sensors are generally sensitive to humidity [23]. In order to understand the effects of water on the sensing characteristics of Sb-SnO_2 nanopowders, it is necessary to recall in brief the behavior of H_2O molecules adsorbed on the surface of metal oxide semiconductors. Water is a donor type molecule and giving one electron to the bulk becomes positively charged, and this leads to the formation of a negative space charge region; moreover, the adsorbed water molecules can dissociate into hydroxyl groups [24]. At low temperature this latter mechanism is slower than previous, but it gains importance increasing the temperature. In any case, humidity interferes with sensor operation because these mechanisms can lead to remarkable temporary or irreversible change in the sensor resistance with time (drift), complicating the detection of the gas target [25].

For accurate and reliable detection with our devices, it is then necessary to observe what effects relative humidity has upon the selective detection of NO_2 gas. Therefore, an experimentation with various RH concentrations was carried out to examine the effects of relative humidity on pure and Sb-promoted devices. Results collected in all ranges of temperature investigated have shown that the sensor resistance decreases as RH increases. As an example, the dynamic response of the sensors at the operating temperature of 200°C to step changes in relative humidity levels is reported in Figure 8. The magnitude of signal increases with increasing RH, as reported in Figure 9 for both sensors investigated. It can be observed that the response to humidity is higher for the SnO_2-based sensor. This could be due to a different texture (in terms of surface area, pore size distribution, etc.) between the two sensing layers. Interestingly, this leads on the Sb-promoted device to a water response almost negligible. Therefore, it can be concluded that water vapor affects less the Sb-doped sensor, and this is advantageous because of the consequent stability of the sensor against ambient humidity fluctuations under practical working conditions for NO_2 monitoring.

4. Conclusions

SnO_2 nanopowders pure and promoted with 5 wt% of antimony were prepared by wet chemical methods and widely characterized by SEM, TEM, XRD, and XPS techniques.

The sensing characteristics of thick film resistive sensors fabricated by the pure SnO_2- and Sb-promoted sensors for the monitoring of trace level of NO_2 were studied. The attention was focused on the Sb-promoted tin oxide film, which has shown interesting properties as NO_2 sensor. Indeed, besides it resulted less sensitive to gas target with respect to the SnO_2 sensor, its sensing properties are not influenced by humidity. By optimizing the operating conditions, an NO_2 sensor with good sensitivity and negligible water influence has been developed.

References

[1] N. Yamazoe, "Toward innovations of gas sensor technology," *Sensors and Actuators B*, vol. 108, no. 1-2, pp. 2–14, 2005.

[2] K. Takahata, *Tin Dioxide Sensors—Development and Applications. Chemical Sensor Technology*, vol. 1, Elsevier, Amsterdam, The Netherlands, 1988.

[3] N. S. Baik, G. Sakai, N. Miura, and N. Yamozoe, "Hydrothermally treated sol solution of tin oxide for thin-film gas sensor," *Sensors and Actuators B*, vol. 63, pp. 74–79, 2000.

[4] Z. Han, N. Guo, F. Li, W. Zhang, H. Zhao, and Y. Qian, "Solvothermal preparation and morphological evolution of stannous oxide powders," *Materials Letters*, vol. 48, no. 2, pp. 99–103, 2001.

[5] K. C. Song and J. H. Kim, "Synthesis of high surface area tin oxide powders via water-in-oil microemulsions," *Powder Technology*, vol. 107, no. 3, pp. 268–272, 2000.

[6] C. H. Shek, J. K. L. Lai, and G. M. Lin, "Grain growth in nanocrystalline SnO_2 prepared by sol-gel route," *Nanostructured Materials*, vol. 11, no. 7, pp. 887–893, 1999.

[7] D. Briand, M. Labeau, J. F. Currie, and G. Delabouglise, "Pd-doped SnO_2 thin films deposited by assisted ultrasonic spraying CVD for gas sensing: selectivity and effect of annealing," *Sensors and Actuators B*, vol. 48, no. 1–3, pp. 395–402, 1998.

[8] N. Pinna and M. Niederberger, "Surfactant-free nonaqueous synthesis of metal oxide nanostructures," *Angewandte Chemie International Edition*, vol. 47, no. 29, pp. 5292–5304, 2008.

[9] D. Zhang, Z. Deng, J. Zhang, and L. Chen, "Microstructure and electrical properties of antimony-doped tin oxide thin film deposited by sol-gel process," *Materials Chemistry and Physics*, vol. 98, no. 2-3, pp. 353–357, 2006.

[10] S.-Y. Lee and B.-O. Park, "Structural, electrical and optical characteristics of SnO_2:Sb thin films by ultrasonic spray pyrolysis," *Thin Solid Films*, vol. 510, no. 1-2, pp. 154–158, 2006.

[11] C. Xu, J. Tamaki, N. Miura, and N. Yamazoe, "Grain size effects on gas sensitivity of porous SnO_2-based elements," *Sensors and Actuators B*, vol. 3, no. 2, pp. 147–155, 1991.

[12] S. G. Ansari, P. Boroojerdian, S. R. Sainkar, R. N. Karekar, R. C. Aiyer, and S. K. Kulkarni, "Grain size effects on H_2 gas sensitivity of thick film resistor using SnO_2 nanoparticles," *Thin Solid Films*, vol. 295, no. 1-2, pp. 271–276, 1997.

[13] G. Korotcenkov, "Gas response control through structural and chemical modification of metal oxide films: state of the art and approaches," *Sensors and Actuators B*, vol. 107, no. 1, pp. 209–232, 2005.

[14] N. Pinna, G. Neri, M. Antonietti, and M. Niederberger, "Non-aqueous synthesis of nanocrystalline semiconducting metal oxides for gas sensing," *Angewandte Chemie International Edition*, vol. 43, no. 33, pp. 4345–4349, 2004.

[15] G. Neri, A. Bonavita, G. Rizzo, et al., "Towards enhanced performances in gas sensing: SnO_2 based nanocrystalline oxides application," *Sensors and Actuators B*, vol. 122, no. 2, pp. 564–571, 2007.

[16] M. M. H. Bhuiyan, S. Katsuki, T. Ueda, and T. Ikegami, "Improvement in the sensitivity of SnO_2 thin film based NO_x gas sensor by loading with single-walled carbon nanotube prepared by pulsed laser deposition process," *Sensor Letters*, vol. 6, no. 4, pp. 635–640, 2008.

[17] F. J. Gutierrez, L. Ares, J. I. Robla, et al., "NO_x tin dioxide sensors activities, as a function of doped materials and temperature," *Sensors and Actuators B*, vol. 16, no. 1–3, pp. 354–356, 1993.

[18] G. Williams and G. S. V. Coles, "NO_x response of tin dioxide based gas sensors," *Sensors and Actuators B*, vol. 16, no. 1–3, pp. 349–353, 1993.

[19] T. Krishnakumar, N. Pinna, K. P. Kumari, K. Perumal, and R. Jayaprakash, "Microwave-assisted synthesis and characterization of tin oxide nanoparticles," *Materials Letters*, vol. 62, no. 19, pp. 3437–3440, 2008.

[20] T. Krishnakumar, R. Jayaprakash, N. Pinna, A. R. Phani, M. Passacantando, and S. Santucci, "Structural, optical and electrical characterization of antimony-substituted tin oxide nanoparticles," *Journal of Physics and Chemistry of Solids*, vol. 70, pp. 993–999, 2009.

[21] E. C. P. E. Rodrigues and P. Olivi, "Preparation and characterization of Sb-doped SnO_2 films with controlled stoichiometry from polymeric precursors," *Journal of Physics and Chemistry of Solids*, vol. 64, no. 7, pp. 1105–1112, 2003.

[22] T. Siciliano, A. Tepore, G. Micocci, A. Genga, M. Siciliano, and E. Filippo, "Transition from n- to p-type electrical conductivity induced by ethanol adsorption on α-tellurium dioxide nanowires," *Sensors and Actuators B*, vol. 138, no. 1, pp. 207–213, 2009.

[23] M. Batzill and U. Diebold, "The surface and materials science of tin oxide," *Progress in Surface Science*, vol. 79, no. 2–4, pp. 47–154, 2005.

[24] F. Réti, M. Fleischer, J. Gerblinger, et al., "Comparison of the water effect on the resistance of different semiconducting metal oxides," *Sensors and Actuators B*, vol. 26, no. 1–3, pp. 103–107, 1995.

[25] N. Bârsan and R. Ionescu, "The mechanism of the interaction between CO and an SnO_2 surface: the role of water vapour," *Sensors and Actuators B*, vol. 12, no. 1, pp. 71–75, 1993.